Structural properties of electrons in quantum dots in high magnetic fields: Crystalline character of cusp states and excitation spectra

Constantine Yannouleas* and Uzi Landman†
School of Physics, Georgia Institute of Technology, Atlanta, Georgia 30332-0430, USA
(Received 17 August 2004; revised manuscript received 4 October 2004; published 15 December 2004)

The crystalline or liquid character of the downward cusp states in *N*-electron parabolic quantum dots at high magnetic fields is investigated using conditional probability distributions obtained from exact diagonalization. These states are of crystalline character for fractional fillings covering both low and high values, unlike the liquid Jastrow-Laughlin wave functions, but in remarkable agreement with the rotating-Wigner-molecule ones [Phys. Rev. B **66**, 115315 (2002)]. The crystalline arrangement consists of concentric polygonal rings that rotate independently of each other, with the electrons on each ring rotating coherently. We show that the rotation stabilizes the Wigner molecule relative to the *static* one defined by the broken-symmetry unrestricted-Hartree-Fock solution. We discuss the nonrigid behavior of the rotating Wigner molecule and pertinent features of the excitation spectrum, including the occurrence of a gap between the ground and first-excited states that underlies the incompressibility of the system. This leads us to conjecture that the rotating crystal (and not the static one) remains the relevant ground state for low fractional fillings even at the thermodynamic limit.

DOI: 10.1103/PhysRevB.70.235319 PACS number(s): 73.21.La, 71.45.Gm, 71.45.Lr

I. INTRODUCTION

The excitation energy spectrum of a two-dimensional *N*-electron semiconductor quantum dot (QD), plotted as a function of angular momentum for a given high magnetic field (B), exhibits downward cusps[1–5] at certain magic angular momenta (L_m), corresponding to states with enhanced stability. For a given value of B, one of these L_m's corresponds to the global minimum of the energy, that is to the ground state (the ground-state value of L_m is denoted as $L_{\rm gs}$). Varying the magnetic field causes the ground state and its angular momentum $L_{\rm gs}$ to change. We note that due to their enhanced stability, only cusp states can become ground states. Underlying these properties is the inherent incompressibility of the cusp states in response to an external magnetic field. As a result, the cusp states have been long recognized[1,3–7] as the finite-N precursors of the fractional quantum Hall states in extended systems. In particular, the fractional fillings ν (defined in the thermodynamic limit) are related to the magic angular momenta of the finite-N system as follows:[8]

$$\nu = \frac{N(N-1)}{2L_m}. \tag{1}$$

(Henceforth, we will drop the subscript m, unless necessary.)

In the literature of the fractional quantum Hall effect (FQHE), ever since the celebrated paper[9] by Laughlin in 1983, the cusp states have been considered to be the antithesis of the Wigner crystal and to be described accurately by liquidlike wave functions, such as the Jastrow-Laughlin[9,10] (JL) and composite-fermion[11,12] (CF) ones. This view, however, has been recently challenged[4,5] by the explicit derivation of trial wave functions for the cusp states that are associated with a rotating Wigner (or electron) molecule, RWM. As we discussed[4,5] earlier, the parameter-free RWM wave functions,[13] which are by construction *crystalline* in character, promise to provide a simpler, but yet improved and more consistent description of the properties of the cusp states, in particular for high angular momenta (corresponding to low fractional fillings).

Issues pertaining to the liquid or crystalline character of the cusp states are significant in both the fields of QD's and the FQHE. Since the many-body wave functions in the lowest Landau level (high B) obtained from exact diagonalization (EXD), the RWM wave functions, and the CF/JL ones have good angular momenta[7] $L > L_0 = N(N-1)/2$, their electron densities are *circularly* symmetric. Therefore investigation of the crystalline or liquid character of these states requires examination of the conditional probability distributions (CPD's, i.e., the fully anisotropic pair correlation functions). These calculations were performed here under high magnetic field conditions for QD's (in a disk geometry[14]) with $N=6-9$ electrons, and for an extensive range of angular momenta. This allowed us to conclude that in all instances examined here (corrresponding to $0.467 > \nu > 0.111$) the cusp states exhibit an unmistakably crystalline character, in contrast to the long held perception in the FQHE literature, with the RWM yielding superior agreement with the exact-diagonalization results.[15] Furthermore, the RWM states are found to be energetically stabilized (i.e., exhibit gain in correlation energy) with respect to the corresponding *static* (symmetry-broken) Wigner molecules, from which the multideterminantal RWM wave functions are obtained through an angular-momentum projection.[16] We will present arguments that allow us to conjecture that the stabilization energy of the cusp states in high B remains nonvanishing even in the thermodynamic limit.

In the beginning of Sec. II, we display the Hamiltonian of the system under consideration and define the conditional probability distributions. Subsequently, in the same section, we present our main results pertaining to the structural properties of the CPD's. Possible improvementes of the RWM wave functions are discussed in Sec. II C. In Sec. III, we recapitulate the essential aspects of the two-step method of symmetry breaking and symmetry restoration, calculate sta-

bilization energies for the RWM, and discuss pertinent features of its excitation spectrum (in particular, the occurrence of a gap between the ground state and the first excited state that is not a mere consequence of finite size; the appearance of this gap underlies the incompressibility of the system). A discussion pertaining to implications for the thermodynamic limit is presented in Sec. IV. Finally, a summary is given in Sec. V.

II. CONDITIONAL PROBABILITY DISTRIBUTIONS

We are interested in wave functions which are exact solutions (or good approximations to them) of the two-dimensional many-body problem defined by the Hamiltonian

$$H=\sum_{i=1}^{N}\frac{1}{2m^*}\left(\mathbf{p}_i-\frac{e}{c}\mathbf{A}_i\right)^2+\sum_{i=1}^{N}\frac{m^*}{2}\omega_0^2\mathbf{r}_i^2+\sum_{i=1}^{N}\sum_{j>i}^{N}\frac{e^2}{\kappa r_{ij}}, \tag{2}$$

which describes N electrons (interacting via a Coulomb repulsion) confined in a parabolic potential of frequency ω_0 and subjected to a perpendicular magnetic field B, whose vector potential is given in the symmetric gauge by

$$\mathbf{A}(\mathbf{r})=\tfrac{1}{2}\mathbf{B}\times\mathbf{r}=\tfrac{1}{2}(-By,Bx,0); \tag{3}$$

m^* is the effective electron mass, κ is the dielectric constant of the semiconductor material, and $r_{ij}=|\mathbf{r}_i-\mathbf{r}_j|$. For sufficiently high magnetic field values (i.e., in the FQHE regime), the electrons are fully spin polarized and the Zeeman term (not shown here) does not need to be considered.

In the $B\to\infty$ limit, the external confinement ω_0 can be neglected, and H can be restricted to operate in the lowest Landau level (LLL), reducing to the form

$$H_{\mathrm{LLL}}=N\frac{\hbar\omega_c}{2}+\sum_{i=1}^{N}\sum_{j>i}^{N}\frac{e^2}{\kappa r_{ij}}, \tag{4}$$

where $\omega_c=eB/(m^*c)$ is the cyclotron frequency.

For finite N, the solutions to the Schrödinger equations corresponding to the Hamiltonians (2) and (4) must have a good angular momentum L. As described by us in detail in Refs. 4, 5, 16, and 17 (see also Sec. III below), these solutions can be well approximated by a two-step method of symmetry breaking at the unrestricted Hartree-Fock (UHF) level and of subsequent symmetry restoration via post-Hartree-Fock projection techniques. As elaborated in our earlier work,[4,5,16,17] the two-step method describes the formation and properties of rotating Wigner molecules in QD's.

As indicated in the Introduction, probing of structural characteristics in many-body wave functions with good angular momentum L requires the use of the conditional probability distributions defined by

$$P(\mathbf{r},\mathbf{r}_0)=\langle\Phi_L|\sum_{i=1}^{N}\sum_{j\neq i}^{N}\delta(\mathbf{r}_i-\mathbf{r})\,\delta(\mathbf{r}_j-\mathbf{r}_0)|\Phi_L\rangle/\langle\Phi_L|\Phi_L\rangle. \tag{5}$$

Here $\Phi_L(\mathbf{r}_1,\mathbf{r}_2,\ldots,\mathbf{r}_N)$ denotes the many-body wave function under consideration. In this paper, we calculate the CPD's for three types of many-body wave functions defined in the lowest Landau level: (*i*) the analytic rotating Wigner molecule wave function, Φ_L^{RWM} (see also Sec. III); (*ii*) the wave function Φ_L^{EXD} obtained through exact diagonalization in the lowest Landau level; and (*iii*) the Jastrow-Laughlin functions Φ_L^{JL}.

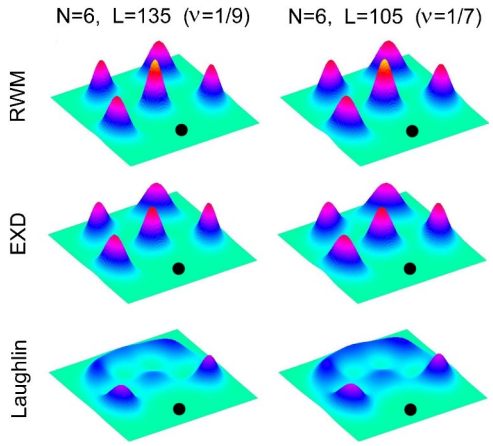

FIG. 1. (Color online) Conditional probability distributions at high B for $N=6$ electrons with $L=135$ ($\nu=\frac{1}{9}$, left column) and $L=105$ ($\nu=\frac{1}{7}$, right column). Top row: RWM case. Middle row: The case of exact diagonalization. Bottom row: The Jastrow-Laughlin case. It is apparent that the exact diagonalization and RWM wave functions have a pronounced crystalline character, corresponding to the (1,5) polygonal configuration of the rotating Wigner molecule. In contrast, the Jastrow-Laughlin wave functions fail to capture this crystalline character, exhibiting a rather "liquid" character. The observation point (identified by a solid dot) was placed at the maximum of the outer ring of the radial electron density (Ref. 4 and 5) of the EXD wave function, namely at $r_0=7.318l_B$ for $L=135$ and $r_0=6.442l_B$ for $L=105$. Here, $l_B=(\hbar c/eB)^{1/2}$. The EXD Coulomb interaction energies (in the lowest Landau level) are 1.6305 and 1.8533 $e^2/\kappa l_B$ for $L=135$ and $L=105$, respectively. The errors relative to the corresponding EXD energies and the overlaps of the trial functions with the EXD ones are (i) for $L=135$, RWM: 0.34%, 0.860; JL: 0.50%, 0.665 and (ii) for $L=105$, RWM: 0.48%, 0.850; JL: 0.46%, 0.710.

$P(\mathbf{r},\mathbf{r}_0)$ is proportional to the conditional probability of finding an electron at $\mathbf{r}$ under the condition that a second electron is located at $\mathbf{r}_0$. This quantity positions the observer on the moving (intrinsic) frame of reference specified by the collective (coherent) rotations that are associated with the good angular momenta of the cusp states.

A. Crystallinity in lower fractions $\frac{1}{9}\leqslant\nu\leqslant\frac{1}{5}$

The CPD's for cusp states corresponding to a lower filling factor than $\nu=\frac{1}{5}$, calculated for $N=6$ electrons with $L=135$ ($\nu=\frac{1}{9}$, left column) and for $N=6$ with $L=105$ ($\nu=\frac{1}{7}$, right column), are displayed in Fig. 1. Figure 2 displays the CPD's for the cusp states with $N=6$ electrons and $L=75$ ($\nu=\frac{1}{5}$, left column) and $N=7$ and $L=105$ ($\nu=\frac{1}{5}$, right column). In both figures, the top row depicts the RWM case. The EXD case is given by the middle row, while the CF cases (which reduce to the JL wave functions for these fractions) are given by the bottom row.

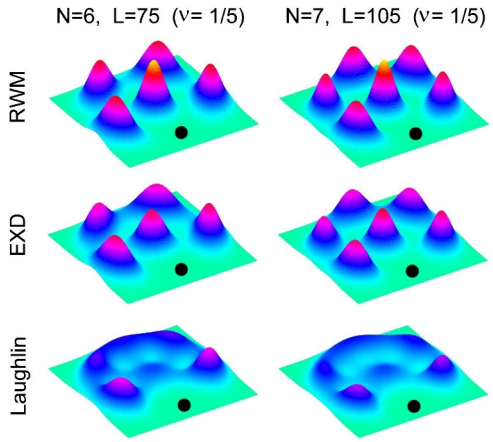

FIG. 2. (Color online) Conditional probability distributions at high B for $N=6$ electrons and $L=75$ ($\nu=\frac{1}{5}$, left column) and for $N=7$ electrons and $L=105$ (again $\nu=\frac{1}{5}$, right column). Top row: RWM case. Middle row: The case of exact diagonalization. Bottom row: The Jastrow-Laughlin case. The exact diagonalization and RWM wave functions have a pronounced crystalline character, corresponding to the (1,5) polygonal configuration of the RWM for $N=6$, and to the (1,6) polygonal configuration for $N=7$. In contrast, the Jastrow-Laughlin wave functions exhibit a characteristic liquid profile that depends smoothly on the number N of electrons. The observation point (identified by a solid dot) is located at $r_0=5.431l_B$ for $N=6$ and $L=75$ and $r_0=5.883l_B$ for $N=7$ and $L=105$. The EXD Coulomb interaction energies (lowest Landau level) are 2.2018 and 2.9144 $e^2/\kappa l_B$ for $N=6$, $L=75$ and $N=7$, $L=105$, respectively. The errors relative to the corresponding EXD energies and the overlaps of the trial functions with the EXD ones are (i) for $N=6$, $L=75$, RWM: 0.85%, 0.817; JL: 0.32%, 0.837 and (ii) for $N=7$, $L=105$, RWM: 0.59%, 0.842; JL: 0.55%, 0.754.

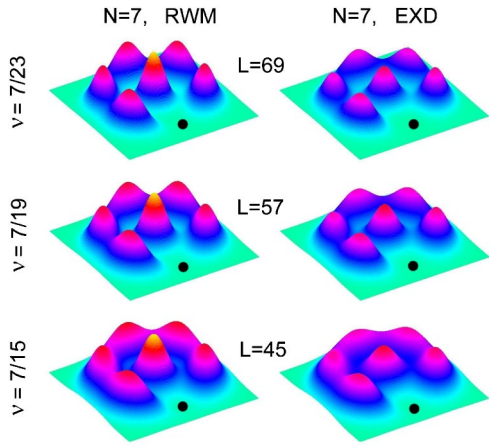

FIG. 3. (Color online) Conditional probability distributions at high B for $N=7$ electrons and $L=69$ ($\nu=\frac{7}{23}=0.304>\frac{1}{5}$, top row), $L=57$ ($1>\nu=\frac{7}{19}=0.368>\frac{1}{3}$, middle row), and $L=45$ ($1>\nu=\frac{7}{15}=0.467>\frac{1}{3}$, bottom row). RWM case: Left column. The case of exact diagonalization is depicted in the right column. Even for these low magic angular momenta (high fractional fillings), both the exact-diagonalization and RWM wave functions have a pronounced crystalline character [corresponding to the (1,6) polygonal configuration of the RWM for $N=7$ electrons]. The observation point (identified by a solid dot) is located at $r_0=4.752l_B$ for $L=69$, $r_0=4.278l_B$ for $L=57$, and $r_0=3.776l_B$ for $L=45$.

There are three principal conclusions that can be drawn from an inspection of Figs. 1 and 2.

(i) The character of the EXD states is unmistakably crystalline with the EXD CPD's exhibiting a well developed molecular polygonal configuration [(1,5) for $N=6$ and (1,6) for $N=7$, with one electron at the center], in agreement with the explicitly crystalline RWM case.

(ii) For all the examined instances (covering the fractional fillings $\frac{1}{9}$, $\frac{1}{7}$, and $\frac{1}{5}$), the JL wave functions fail to capture the intrinsic crystallinity of the EXD states. In contrast, they represent "liquid" states in agreement with an analysis that goes back to the original papers[9,10] by Laughlin. In particular, Ref. 10 investigated the character of the JL states through the use of a pair correlation function [usually denoted by $g(R)$] that determines the probability of finding another electron at the absolute relative distance $R=|\mathbf{r}-\mathbf{r}_0|$ from the observation point $\mathbf{r}_0$. Our anisotropic CPD of Eq. (5) is of course more general (and more difficult to calculate) than the $g(R)$ function of Ref. 10. However, both our $P(\mathbf{r},\mathbf{r}_0)$ (for $N=6$ and $N=7$ electrons) and the $g(R)$ (for $N=1000$ electrons, and for $\nu=\frac{1}{3}$ and $\nu=\frac{1}{5}$) in Ref. 10 reveal a similar characteristic liquid like and short-range-order behavior for the JL states, eloquently described in Ref. 10 (see pp. 249 and 251). Indeed, we remark that only the first-neighbor electrons on the outer rings can be distinguished as separate localized electrons in our CPD plots of the JL functions (see Figs. 1 and 2).

(iii) For a finite number of electrons, pronounced crystallinity of the EXD states occurs already at the rather high $\nu=\frac{1}{5}$ value (see Fig. 2). This finding is particularly interesting in light of expectations[18] (based on comparisons[9,10,19] between the JL states and the static bulk Wigner crystal) that a liquid-to-crystal phase transition may take place only at lower fillings with $\nu\leqslant\frac{1}{7}$.

B. Crystallinity in higher fractions $\frac{1}{5}<\nu<1$

Following the conclusion that the crystalline character of the cusp states in QDs is already well developed for fractional fillings with the unexpected high value of $\nu=\frac{1}{5}$, a natural question arises concerning the presence or absence of crystallinity in cusp states corresponding to higher fractional fillings, i.e., states with $\frac{1}{5}<\nu<\frac{1}{3}$, and even with $\frac{1}{3}<\nu<1$. To answer this question, we show in Fig. 3 the CPD's for the RWM (left column) and EXD (right column) wave functions for the case of $N=7$ electrons and for $L=69$ $\left(\frac{1}{5}<\nu=\frac{7}{23}<\frac{1}{3}\right)$, $L=57$ $\left(\frac{1}{3}<\nu=\frac{7}{19}<1\right)$, and $L=45$ $\left(\frac{1}{3}<\nu=\frac{7}{15}<1\right)$. Unlike the long held perceptions in the FQHE literature (which were reasserted in two recent publications[18]) the CPD's in Fig. 3 demonstrate that the character of the cusp states with high fractional fillings is not necessarily "liquidlike." Indeed, these high-ν cusp states exhibit a well developed crystallinity associated with the (1,6) polygonal configuration of the RWM, appropriate for $N=7$ electrons.

Of interest also is the case of $\nu=\frac{1}{3}$. Indeed, for this fractional filling, the liquid JL function is expected to provide the best approximation, due to very high overlaps (better than 0.99) with the exact wave function.[20,21] In Fig. 4, we display the CPD's for $N=7$ and $L=63$ $\left(\nu=\frac{1}{3}\right)$, and for the three cases

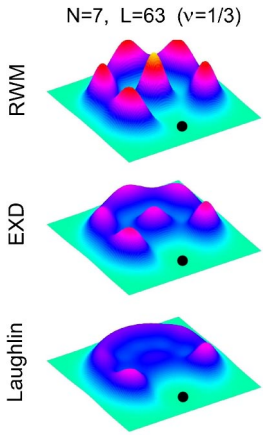

FIG. 4. (Color online) CPD's at high B for $N=7$ and $L=63$ $\left(\nu=\frac{1}{3}\right)$. Top: RWM case. Middle: EXD case. Bottom: JL case. Unlike the JL CPD (which is liquid), the CPD's for the exact-diagonalization and RWM wave functions exhibit a well developed crystalline character [corresponding to the (1,6) polygonal configuration of the RWM for $N=7$ electrons]. The observation point (identified by a solid dot) is located at $r_0=4.568l_B$.

of RWM, EXD, and JL wave functions. Again, even in this most favorable case, the CPD of the JL function disagrees with the EXD one, which exhibits clearly a (1,6) crystalline configuration in agreement with the RWM CPD.

Similar crystalline correlations at higher fractions were also found for QDs of a different size, e.g., with $N=6$, $N=8$, and $N=9$ electrons. As illustrative examples for these additional sizes, we display in Fig. 5 the CPD's for $N=8$ and $L=91$ $\left(\frac{1}{5}<\nu=\frac{4}{13}<\frac{1}{3}\right)$ and for $N=9$ and $L=101$ $\left(\frac{1}{3}<\nu=\frac{36}{101}<1\right)$. Again, the CPD's (both for the RWM and the EXD wave functions) exhibit a well developed crystalline character in accordance with the (1,7) and (2,7) polygonal configurations of the RWM, appropriate for $N=8$ and $N=9$ electrons, respectively.

The case of $N=9$ is of particuler significance. Indeed it represents the smallest number of electrons with a nontrivial concentric-ring arrangement, i.e., the inner ring has more than one electrons. As the two CPD's (reflecting the choice of taking the observation point [$\mathbf{r}_0$ in Eq. (5)] on the outer or the inner ring) for $N=9$ reveal, the polygonal electron rings rotate *independently* of each other. Thus, e.g., to an observer located on the inner ring, the outer ring will appear as uniform, and vice versa. The fact that both the RWM and exact wave functions share this property of independently rotating rings is a testament to the ability of the RWM theory to capture the essential physics of QD's in high B.

C. Improvements of the RWM wave functions

It is of importance to note here that the favorable comparison between the crystalline structure of the RWM and that of the exact wave functions, in contrast to the liquidlike character of the JL functions, persists even for cases where the latter is found to have the advantage (over the RWM) concerning total energies and wave function overlaps. As examples, we refer to the case of $\nu=\frac{1}{5}$ discussed in the caption of Fig. 2 (see in particular the errors in the energies for the RWM and JL functions relative to the exact energies given at the end of the caption).

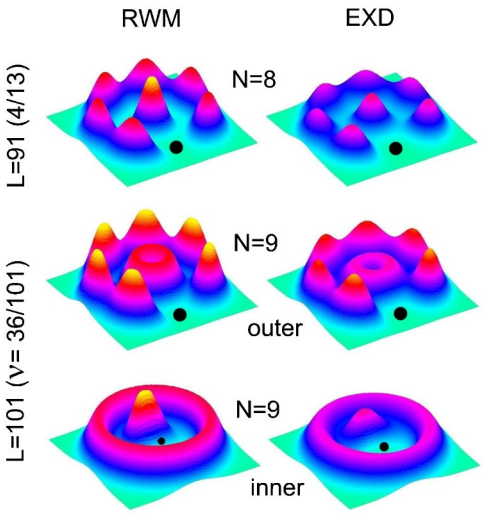

FIG. 5. (Color online) Additional CPD's at high B. RWM results: Left column. Results from exact diagonalization are depicted on the right column. Top row: $N=8$ electrons and $L=91$ $\left(\frac{1}{5}<\nu=\frac{4}{13}=0.308<\frac{1}{3}\right)$. Two bottom rows: $N=9$ electrons and $L=101$ $\left(\frac{1}{3}<\nu=\frac{36}{101}=0.356<1\right.$, see text for explanation). Even for these low magic angular momenta (high fractional fillings), both the exact-diagonalization and RWM wave functions have a pronounced crystalline character [corresponding to the (1,7) and (2,7) polygonal configurations of the RWM for $N=8$ and 9 electrons]. The observation point (identified by a solid dot) is located at $r_0=5.105l_B$ for $N=8$, $L=91$, and $r_0=5.218l_B$ (outer) and $r_0=1.662l_B$ (inner) for $N=9$, $L=101$.

Close inspection of the humps in the CPD's obtained from the RWM and through exact diagonalization reveals that the RWM tends to somewhat overestimate the degree of crystallinity, i.e., the RWM humps are narrower and higher (this tendency diminishes for larger values of L). Nevertheless, the degree of overall agreement between the exact results and those obtained through the *parameter-free* RWM wave functions is rather remarkable. Moreover, the high level of agreement between the RWM and exact results extends to other properties. This includes the zeroes (often called vortices) of the many-body wave functions. Indeed, as recently shown in Ref. 22, the exact wave functions (in contrast to the JL ones) have *simple zeroes* whose topology is in agreement with that of the simple zeroes of the RWM functions.

The above suggest that the RWM wave functions can form the nucleus for constructing a whole class of rotating crystalline functions with added variational freedom, which will yield further quantitative energetic and structural improvements. For example, the RWM functions could be used as the basis for constructing variational wave functions in diffusion[23] and variational[24] quantum Monte Carlo studies. For a most recent investigation along these lines, see Ref. 25, where our RWM function is augmented by a Jastrow prefactor with an exponent that is treated variationally. We remark, however, that the variational wave function employed in Ref. 25 has multiple zeroes due to the Jastrow factor, in disagreement with the exact diagonalization results.

III. RESTORATION OF CIRCULAR SYMMETRY

A. Correlated many-body wave functions

Our two-step method for deriving the RWM wave function is anchored in the distinction[17] between a *static* and a *rotating* Wigner molecule, with the rotation stabilizing the latter relative to the former. Further elaboration on this point requires generation of global ground states out of the cusp states, achieved through inclusion[6,17] of an external parabolic confinement (of frequency ω_0). In the two-step method, the static WM is first described by an unrestricted Hartree-Fock (UHF) determinant that violates the circular symmetry.[26] Subsequently, the rotation of the WM is described by a post-Hartree-Fock step of restoration of the broken circular symmetry via projection techniques.[16] We note that, in the limit $N\rightarrow\infty$, the static WM of the UHF develops to the extended two-dimensional Wigner crystal[27] and its more sophisticated variants.[19]

In general, the localized broken symmetry orbitals of the HF determinant are determined numerically via a self-consistent solution of the UHF equations. Since we focus here on the case of high B, we can approximate the UHF orbitals (first step of our procedure) by (parameter free) displaced Gaussian functions; namely, for an electron localized at $\mathbf{R}_j$ (Z_j), we use the orbital

$$u(z,Z_j)=\frac{1}{\sqrt{\pi}\lambda}\exp\left(-\frac{|z-Z_j|^2}{2\lambda^2}-i\varphi(z,Z_j;B)\right), \qquad (6)$$

with $\lambda=\sqrt{\hbar/m^*\Omega}$, $\Omega=\sqrt{\omega_0^2+\omega_c^2/4}$, where $\omega_c=eB/(m^*c)$ is the cyclotron frequency. We have used complex numbers to represent the position variables, so that $z=x+iy$, $Z_j=X_j+iY_j$. The phase guarantees gauge invariance in the presence of a perpendicular magnetic field and is given in the symmetric gauge by $\varphi(z,Z_j;B)=(xY_j-yX_j)/2l_B^2$, with $l_B=\sqrt{\hbar c/eB}$. We only consider the case of fully polarized electrons, which is appropriate at high B.

We take the Z_j's to coincide with the equilibrium positions [forming a structure of r concentric regular polygons denoted as $(n_1,n_2,\ldots,n_r)$] of $N=\Sigma_{q=1}^{r}n_q$ classical point charges inside an external parabolic confinement of frequency ω_0. Then we proceed to construct the UHF determinant $\Psi^{\mathrm{UHF}}[z]$ out of the orbitals $u(z_i,Z_i)$'s, $i=1,\ldots,N$. Correlated many-body states with good total angular momenta L can be extracted[5,16] from the UHF determinant using projection operators, i.e.,

$$\Phi_L^{\mathrm{RWM}}=\int_0^{2\pi}\cdots\int_0^{2\pi}d\gamma_1\cdots d\gamma_r \times\Psi^{\mathrm{UHF}}(\gamma_1,\ldots,\gamma_r)\exp\left(i\sum_{q=1}^{r}\gamma_qL_q\right), \qquad (7)$$

where $L=\Sigma_{q=1}^{r}L_q$ and $\Psi^{\mathrm{UHF}}[\gamma]$ is the original UHF determinant with *all the orbitals of the qth ring* rotated (collectively, i.e., coherently) by the *same* azimuthal angle γ_q, and each ring is rotated independently of each other. Note that Eq. (7) can be written as a product of projection operators acting on the original UHF determinant [i.e., $\Psi^{\mathrm{UHF}}(\gamma_1=0,\ldots,\gamma_r=0)$, see Eqs. (6) and (7) in Ref. 5]. Setting $\lambda=l_B\sqrt{2}$ restricts the orbital in Eq. (6) to lie entirely in the lowest Landau level, and allows for the derivation of the analytic RWM functions.[5] We stress that while the initial trial wave function of the UHF equations consists of a single determinant, the projected wave function is a linear superposition of many determinants, as can be explicitly seen from the analytic forms of the RWM functions in Ref. 5.

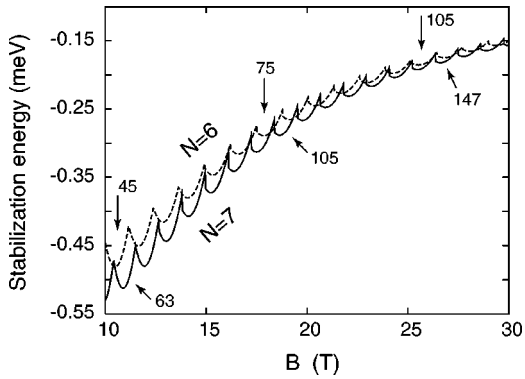

FIG. 6. Stabilization energies $\Delta E_{\mathrm{gs}}^{\mathrm{gain}}$ for $N=6$ (dashed curve) and $N=7$ (solid curve) fully polarized electrons in a parabolic QD as a function of B. The troughs associated with the major fractional fillings ($\frac{1}{3}$, $\frac{1}{5}$, and $\frac{1}{7}$) and the corresponding ground-state angular momenta [see Eq. (1)] are indicated with arrows. We have extended the calculations up to $B=120$ T (not shown), and verified that $\Delta E_{\mathrm{gs}}^{\mathrm{gain}}$ remains negative while its absolute value vanishes as $B\rightarrow\infty$. The choice of parameters is $\hbar\omega_0=3$ meV (parabolic confinement), $m^*=0.067m_e$ (electron effective mass), and $\kappa=12.9$ (dielectric constant).

B. Stabilization energy

In the case of finite B (requiring the inclusion of confinement, i.e., $\omega_0\neq 0$), the projected energy corresponding to a symmetry-restored RWM state with angular momentum L is given [in the case of a single $(0,N)$ or a $(1,N-1)$ ring] by[16,17]

$$E_{\mathrm{PRJ}}(L)=\int_0^{2\pi}h(\gamma)e^{i\gamma L}d\gamma\Big/\int_0^{2\pi}n(\gamma)e^{i\gamma L}d\gamma, \qquad (8)$$

with $h(\gamma)=\langle\Psi^{\mathrm{UHF}}(0)|H|\Psi^{\mathrm{UHF}}(\gamma)\rangle$ and $n(\gamma)=\langle\Psi^{\mathrm{UHF}}(0)|\Psi^{\mathrm{UHF}}(\gamma)\rangle$, where $\Psi^{\mathrm{UHF}}(\gamma)$ is the original UHF determinant with *all the orbitals* rotated (collectively) by the *same* azimuthal angle γ. H is the many-body Hamiltonian in Eq. (2). The UHF energies are simply given by $E_{\mathrm{UHF}}=h(0)/n(0)$.

We note that, unlike the UHF ground state (describing a static Wigner molecule) which does not have good angular momentum, the ground states of the RWM exhibit good angular momenta (labeled as L_{gs}, as aforementioned) that coincide with magic ones [we denote the ground-state energy of the RWM as $E_{\mathrm{PRJ}}^{\mathrm{gs}}\equiv E_{\mathrm{PRJ}}(L_{\mathrm{gs}})$]. Note that in Fig. 6 the ground-state magic angular momenta obey

$$L_{\mathrm{gs}}=N(N-1)/2+k(N-1), \qquad (9)$$

with $k=0,1,2,\ldots,$. Such sequences, having as a period the number of eletrons on the crystalline polygonal ring [5 and 6

for the (1,5) and (1,6) RWMs corresponding to $N=6$ and $N=7$], reflect directly the collective rotation and incompressibilty of the RWM (see Sec. III C).

The stabilization energy, $\Delta E_{\rm gs}^{\rm gain}=E_{\rm PRJ}^{\rm gs}-E_{\rm UHF}$, of the *rotating* WM relative to the *static* one (namely the fact that $E_{\rm PRJ}^{\rm gs}<E_{\rm UHF}$, see Fig. 6) is a purely quantum effect. This energy gain, $\Delta E_{\rm gs}^{\rm gain}$, demonstrated here for $N=6$ and 7 electrons, is in fact a general property of states projected out of trial functions with broken symmetry. This is due to an "energy gain" theorem[28] stating that at least one of the projected states (i.e., the ground state) has an energy lower than that of the original broken-symmetry trial function (e.g., the UHF determinant considered above).

C. Excitation gap

The oscillations of the stabilization energy (Fig. 6) reflect the oscillatory behavior of the energy of the projected RWM states, as well as of the exact ones, since the mean-field energy $E_{\rm UHF}$ varies smoothly with B (see Ref. 17). Underlying the oscillatory behavior of the ground-state energies is a fundamental property of the spectrum of the system, namely, the appearance of special gaps due to the enhanced stability of the cusp states. Indeed, for a given magnetic field, both the ground state (specified by $L_{\rm gs}$), as well as the first excited state (specified by L_1), are magic [with[29] $L_1=L_{\rm gs}\pm(N-1)$ for $N=6-8$]. As an example of this behavior, we display in Fig. 7 the low part of the EXD excitation spectrum for a QD with $N=7$, $B=18.8$ T, $\hbar\omega_0=3$ meV, and $\kappa=12.9$. The states $L=99$, $L=105$ (the ground state), and $L=111$ are demonstrated indeed to be cusp states of enhanced stability (all three states are well separated from the rest of the excited states).

For the given magnetic field $B=18.8$ T, the first excited state corresponds to $L=99$. However, as B increases, we found that the state with $L=111$ diminishes in energy relative to that with $L=99$, becoming itself the first excited state, and eventually (as B is increased further) replacing $L=105$ as the ground state. This sequence of changes occurs for all ground states (with magic angular momenta) accessed through variation of the magnetic field. This results in the behavior of the excitation gap, $\Delta=E^1-E^{\rm gs}$, shown in Fig. 8 [the calculations here were performed with the RWM projected energies of Eq. (8)]. The gap in Fig. 8 separates states with similar internal structure, i.e., they exhibit the same polygonal configuration as revealed through the CPD analysis for $N=7$ electrons (see Figs. 2–4). The internal structures of higher excited states differ from that of the ground state, with the disparity increasing with the excitation energy.

The incompressibility of the cusp states (which, as discussed above, correspond to magic angular momenta) is connected directly to the appearance of the gap (as discussed in the context of the FQHE in Ref. 9). The discussion presented here about the nature of the excitation spectrum (and in particular the existence of a gap Δ) allows us to comment on the influence of impurities and disorder on the properties of the quantum dot. Naturally, we focus on the regime of small or moderate disorder, since a high degree of disorder (or strong impurities) will destroy both the gaps in the spectrum, as well as the coherent (collective) nature of the rotating

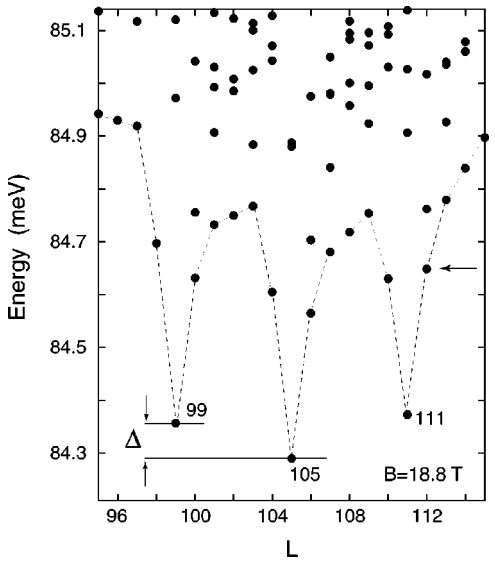

FIG. 7. Low-energy part of the spectrum of the parabolic QD whose parameters are the same as those in Fig. 6, calculated as a function of the angular momentum L through exact diagonalization for $N=7$ electrons with a magnetic field $B=18.8$ T. We show here the spectrum in the interval $95\leqslant L\leqslant 115$ (in the neighborhood of $\nu=\frac{1}{5}$). The magic angular momentum values corresponding to cusp states are marked (99, 105, and 111), and they are seen to be separated from the rest of the spectrum. For the given value of B, the global energy minimum (ground state) occurs for $L_{\rm gs}=105$, and the gap Δ to the first excited state ($L=99$) is indicated. The lowest energies for the different L's in the plotted range are connected by a dashed line, as a guide to the eye. The zero of energy corresponds to $7\hbar\Omega$, where $\Omega=(\omega_0^2+\omega_c^2/4)^{1/2}$ and $\omega_c=eB/(m^*c)$. The horizontal arrow denotes the energy of the Laughlin quasihole at $L=112$. It is seen that the Laughlin quasihole is not the lowest excited state.

Wigner molecule. The effect of disorder (or impurities) depends on the size of the gap. For sufficiently weak disorder, both the excitation gap Δ and the coherence of the magic angular momentum states maintain, namely, the states separated by the gap experience only *local* disorder-induced perturbations (i.e., they broaden) and they remain conducting (see Sec. IV below). Obviously, for cases of a vanishing gap (i.e., between the fractional fillings, see arrows in Fig. 8), even weak disorder can induce a *global* change in the character of the (perturbed) wave functions by strongly mixing the degenerate $L_{\rm gs}$ and L_1 cusp states (and often additional nearby cusp states depending on the magnitude of B), and this can lead to a state with a broken-symmetry electron density having characteristics of a pinned Wigner crystallite.[30]

IV. DISCUSSION: IMPLICATIONS FOR THE THERMODYNAMIC LIMIT

While our focus here is on the behavior of trial and exact wave functions in (finite) QDs in high magnetic fields, it is natural to inquire about possible implications of our findings to FQHE systems in the thermodynamic limit.

We recall that appropriate trial wave functions for clean FQHE systems possess a good angular momentum $L\geqslant L_0$, a

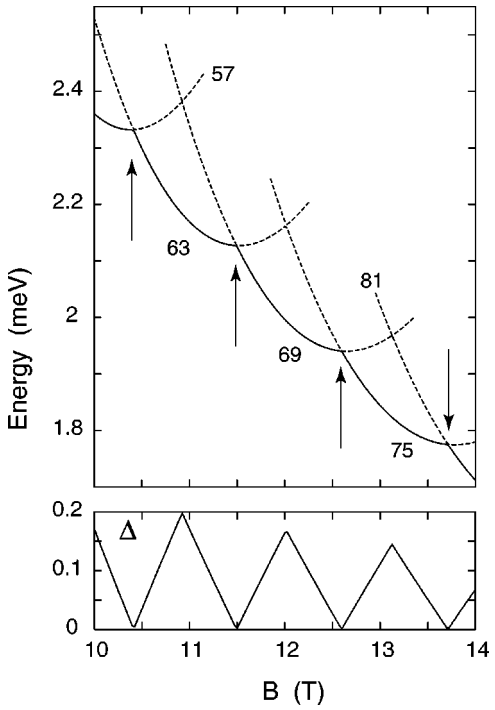

FIG. 8. Top: RWM projected energies [see Eq. (8)] calculated as a function of the magnetic field B for $N=7$ electrons in a parabolic QD with the same parameters as those used in Figs. 6 and 7. Each of the parabolalike curves (made partly of a solid and partly of a dashed line) corresponds to the marked value of the angular momentum—i.e., for the range of magnetic fields shown here, $L_{\mathrm{gs}}=57\ (\frac{7}{19})$, 63 $(\frac{1}{3})$, 69 $(\frac{7}{23})$, 75 $(\frac{7}{25})$, and 81 $(\frac{7}{27})$, with the corresponding value of the fractional filling $\nu=N(N-1)/(2L_{\mathrm{gs}})$ given in parentheses. The solid lines denote the ground-state energies, and the dashed lines give the values of the first-excited-state energies. Note that the gap between the ground and the first excited state, $\Delta=E^{1}-E^{\mathrm{gs}}$, oscillates as a function of B. The arrows denote the values of B for which the gap vanishes, occuring between the fractional fillings. The zero of energy corresponds to $7\hbar\Omega+E_{\mathrm{cl}}^{\mathrm{st}}$, where $\Omega=(\omega_0^2+\omega_c^2/4)^{1/2}$ [with $\omega_c=eB/(m^*c)$] and $E_{\mathrm{cl}}^{\mathrm{st}}$ is the classical energy of the static Wigner molecule (see Ref. 17). Bottom: The gap Δ plotted versus B.

property shared by both the CF/JL and RWM functions.[5,9–11] We also recall the previous finding[31] that for large fractional fillings $\nu>\nu_0$, the liquidlike (and circularly uniform) CF/JL function is in the thermodynamic limit energetically favored compared[9,10,12,19] to the broken-symmetry static Wigner crystal (which has no good angular momentum); for $\nu<\nu_0$, the static Wigner crystal becomes lower in energy. This finding was enabled by the form of the JL functions, which facilitated computations of total energies as a function of size for sufficiently large N (e.g., $N=1000$).

A main finding of this paper is that the *exact-numerical-diagonalization wave functions of small systems* ($N\leqslant 10$) *are crystalline in character for both low and high fractional fillings.* This finding contradicts earlier suggestions[3,9,10,18] that, for high ν's, small systems are accurately described by the liquidlike JL wave functions and their descendants, e.g., the composite-fermion ones. Of course, for the same high ν's, our small-size results cannot exclude the possibility that the CPDs of the exact solution may exhibit with increasing N a transition from crystalline to liquid character, in agreement with the JL function. However, at the moment, the existence of such a transition remains an open theoretical subject.

For the *low fractions*, the RWM theory raises still another line of inquiry. Due to the specific form of the RWM wave functions, computational limitations[32] prevent us at present from making extrapolations of total energies at a given ν as $N\rightarrow\infty$. Nevertheless, from the general theory of projection operators, one can conclude that the RWM energies exhibit a different trend compared to the JL ones, whose energies were found[9,10,12,19] to be higher than the static Wigner crystal. Indeed the rotating-Wigner-molecule wave functions remain lower in energy than the corresponding *static* crystalline state for *all values* of N and ν, even in the thermodynamic limit. This is due to the fact that the aforementioned energy-gain theorem[28] (see Sec. III) applies for any number of electrons N and for all values of the magnetic field B. Naturally, the RWM wave functions will be physically relevant compared to those of the broken-symmetry crystal at the thermodynamic limit if the energy gain does not vanish when $N\rightarrow\infty$; otherwise, one needs to consider the posssibility that the static crystal is the relevant physical picture.

The discussion in the above paragraph may be recapitulated by the following question: which state is the relevant one in the thermodynamic limit ($N\rightarrow\infty$)—the broken-symmetry one (i.e., the static Wigner crystal) or the symmetry restored (i.e., rotating crystal) state? This question, in the context of bulk broken-symmetry systems, has been addressed in the early work of Anderson,[33] who concluded that the broken-symmetry state (here the UHF static crystalline solution) can be safely taken as the effective ground state. In arriving at this conclusion Anderson invoked the concept of (generalized) rigidity. As a concrete example, one would expect a crystal to behave like a *macroscopic* body, whose Hamiltonian is that of a *heavy rigid rotor* with a low-energy excitation spectrum $L^2/2\mathcal{J}$, the moment of inertia $\mathcal{J}$ being of order N (macroscopically large when $N\rightarrow\infty$). The low-energy excitation spectrum of this heavy rigid rotor above the ground-state ($L=0$) is essentially gapless (i.e., continuous). Thus although the formal ground state posseses continuous rotational symmetry (i.e., $L=0$), "there is a manifold of other states, degenerate in the $N\rightarrow\infty$ limit, which can be recombined to give a very stable wave packet with essentially the nature"[34] of the broken-symmetry state (i.e., the static Wigner crystal in our case). As a consequence of the "macroscopic heaviness" as $N\rightarrow\infty$, one has the following: (i) The energy gain due to symmetry restoration (i.e., the stabilization energy $\Delta E_{\mathrm{gs}}^{\mathrm{gain}}$) vanishes as $N\rightarrow\infty$ and (ii) the relaxation of the system from the wave packet state (i.e., the static Wigner crystal) to the symmetrized one (i.e., the rotating crystal) becomes exceedingly long. This picture underlies the aforementioned conclusion that in the thermodynamic limit the broken-symmetry state may be used as the effective ground state.

Consequently, in the following we will focus on issues pertaining to the "rigidity" of the rotating Wigner molecule in high magnetic fields. In particular, using our projection method and exact diagonalization, we demonstrated explicitly in previous publications[17,35] that the rigid-rotor picture

applies to an N-electron QD only when $B=0$. In contrast, in the presence of a high magnetic field, we found[17] that the electrons in the QD do not exhibit global rigidity and therefore cannot be modeled as a macroscopic rotating crystal. Instead, a more appropriate model is that of a *highly nonrigid* rotor whose moment of inertia depends strongly on the value of the angular momentum L.

The nonrigid rotor at high B has several unique properties: (i) The ground state has angular momentum $L_{\rm gs}>0$. (ii) While the rotating electron molecule does not exhibit *global* rigidity, it possesses *azimuthal* rigidity (i.e., all electrons on a given ring rotate coherently), with the rings, however, rotating independently of each other. Furthermore, the radii of the rings vary for different values of L, unlike the case of a rigid rotor (see, for example, the locations of $\mathbf{r}_0$ in Fig. 1 and Fig. 3 for different L values). (iii) The excitation spectra do not vary as L^2; instead they consist of terms that vary as $aL+b/\sqrt{L}$ [for the precise values of the constants a and b in the case of $(0,N)$ or $(1,N-1)$ electron molecules, see Ref. 17]. (iv) The angular momentum values are given by the magic values (see Ref. 5) $L=L_0+\Sigma_{q=1}^{r}k_q n_q$, where $(n_1,n_2,\ldots,n_r)$ is the polygonal ring arrangement of the static Wigner molecule (with n_q the number of electrons on the qth ring) and $k_1<k_2<\cdots<k_r$ are non-negative integers. These magic L's are associated with the cusp states which exhibit a relative energy gain with respect to neighboring excitations. Thus the low-energy excitation spectrum of the nonrigid rotor is not dense and exhibits gaps due to the occurrence of the magic (cusp) states (see Sec. III C). Furthermore, these gaps are reflected in the oscillatory behavior of $\Delta E_{\rm gs}^{\rm gain}$ (see, e.g., Fig. 6) as a function of B (or ν).

As N increases, more polygonal rings are successively added, and since the polygonal rings rotate independently of each other (see, e.g., the case of $N=9$ in Fig. 5), we expect that the non-rigid-rotor picture remains valid even as $N\rightarrow\infty$. As a result, it is plausible to conjecture the following properties at high B in the thermodynamic limit: (i) the oscillatory character of $\Delta E_{\rm gs}^{\rm gain}$ will maintain, yielding nonvanishing stabilization energies at the fractional fillings ν [see Eq. (1)], and (ii) the low-energy excitation spectra of the system will still exhibit gaps in the neighborhood of the magic angular momenta (see Fig. 8). Of course, these conjectures need to be further supported through numerical calculations for large N. Nevertheless, the above discussion indicates that the question of which state is physically relevant for low fractions in the thermodynamic limit at high B, i.e., the broken-symmetry static crystal or the symmetrized rotating crystal, remains open, and cannot be answered solely following the path of Ref. 33.

The rotating Wigner crystal has properties characteristic of FQHE states, i.e., it is incompressible (connected to the presence of an excitation gap) and carries a current[36] (while the broken-symmetry static crystal is insulating). Thus, we may conjecture that a transition at lower fractional fillings from a conducting state with good circular symmetry to an insulating Wigner crystal cannot occur *spontaneously* for clean systems. Therefore, it should be possible to observe FQHE-type behavior at low fractional fillings in a clean system—a prediction that could explain the observations of Ref. 37, where FQHE behavior has been observed for low fractional fillings typically associated with the formation of a static Wigner crystal. In practice, however, impurities and defects may influence the properties of the rotating crystal (and its excitations), depending on the magnitude of the excitation gap discussed in the previous section. Thus one of the main challenges for FQHE observation at such low fillings relates to fabrication of high mobility (nearly impurity-free) samples.[38,39]

V. SUMMARY

In summary, we have carried out the first systematic investigations (for $6\leqslant N\leqslant 9$) of structural properties of cusp states in parabolic quantum dots at high magnetic fields. Our anisotropic conditional probability distributions from exact diagonalization show that these states are crystalline in character for both low and high fractional fillings, unlike the liquidlike Jastrow-Laughlin[9,10] wave functions, but in remarkable agreement with the recently proposed rotating-Wigner-molecule[4,5] ones. The cusp states of N-electron parabolic QDs are precursors to the extended fractional quantum Hall states (and not to the static Wigner crystal) due to stabilization of the *rotating* Wigner molecule (having a good angular momentum) relative to the *static* one (that exhibits broken symmetry). The rotating Wigner molecule in high B does not exhibit global rigidity; instead, it possesses *azimuthal* rigidity (i.e., all electrons on a given ring rotate coherently), with the rings, however, rotating independently of each other.

Furthermore, we demonstrated pertinent features of the spectrum of quantum dots in high B, showing that both the ground state and the first excited state correspond to magic angular momenta (cusp states). For a given B, this leads to the appearance of a special gap that is not a mere consequence of the finite size of the system (and thus it is expected to maintain in the thermodynamic limit, underlying the incompressibility of the electron system). Finally, we discussed in detail issues pertaining to the implications of the rotating-Wigner-molecule theory for FQHE systems at the thermodynamic limit (see Sec. IV).

ACKNOWLEDGMENTS

We thank M. Pustilnik for comments on the manuscript. This research is supported by the U.S. DOE (Grant No. FG05-86ER45234).

*Electronic address: Constantine.Yannouleas@physics.gatech.edu
†Electronic address: Uzi.Landman@physics.gatech.edu

[1] R. B. Laughlin, Phys. Rev. B **27**, 3383 (1983).
[2] P. A. Maksym and T. Chakraborty, Phys. Rev. Lett. **65**, 108 (1990).
[3] J. K. Jain and T. Kawamura, Europhys. Lett. **29**, 321 (1995).
[4] C. Yannouleas and U. Landman, Phys. Rev. B **68**, 035326 (2003).
[5] C. Yannouleas and U. Landman, Phys. Rev. B **66**, 115315 (2002).
[6] S. R. E. Yang, A. H. MacDonald, and M. D. Johnson, Phys. Rev. Lett. **71**, 3194 (1993).
[7] A. L. Jacak, P. Hawrylak, and A. Wojs, *Quantum Dots* (Springer, Berlin, 1998), in particular Chap. 4.5.
[8] S. M. Girvin and T. Jach, Phys. Rev. B **28**, 4506 (1983).
[9] R. B. Laughlin, Phys. Rev. Lett. **50**, 1395 (1983).
[10] R. B. Laughlin, in *The Quantum Hall Effect*, edited by R. E. Prange and S. M. Girvin (Springer, New York, 1987), p. 233.
[11] J. K. Jain, Phys. Rev. B **41**, 7653 (1990).
[12] S. S. Mandal, M. R. Peterson, and J. K. Jain, Phys. Rev. Lett. **90**, 106403 (2003).
[13] In previous publications the RWM wave functions were also referred to as rotating-electron-molecule (REM) wave functions.
[14] The results in Figs. 1–5 were obtained without consideration of a confinement, and they are not influenced (high B) by inclusion of a parabolic confinement [Refs. 3, 6, and 17]. For the influence of the confinement on the energies, see Refs. 3, 6, and 17.
[15] C. Yannouleas and U. Landman, cond-mat/0401610 (unpublished).
[16] C. Yannouleas and U. Landman, J. Phys.: Condens. Matter **14**, L591 (2002); Phys. Rev. B **68**, 035325 (2003).
[17] C. Yannouleas and U. Landman, Phys. Rev. B **69**, 113306 (2004).
[18] G. S. Jeon, C.-C. Chang, and J. K. Jain, J. Phys.: Condens. Matter **16**, L271 (2004); Phys. Rev. B **69**, 241304 (2004).
[19] P. K. Lam and S. M. Girvin, Phys. Rev. B **30**, 473 (1984).
[20] D. Yoshioka, *The Quantum Hall Effect* (Springer, Berlin, 2002), Chap. 4.4.
[21] E. V. Tsiper and V. J. Goldman, Phys. Rev. B **64**, 165311 (2001).
[22] M. B. Tavernier, E. Anisimovas, and F. M. Peeters, Phys. Rev. B **70**, 155321 (2004).
[23] F. Bolton, Phys. Rev. B **54**, 4780 (1996).
[24] A. Harju, S. Siljamäki, and R. M. Nieminen, Phys. Rev. B **60**, 1807 (1999).
[25] C.-C. Chang, G. S. Jeon, and J. K. Jain, cond-mat/0406744 (unpublished).
[26] C. Yannouleas and U. Landman, Phys. Rev. Lett. **82**, 5325 (1999); Phys. Rev. B **61**, 15895 (2000).
[27] D. J. Yoshioka and P. A. Lee, Phys. Rev. B **27**, 4986 (1983).
[28] See Sec. III in P.-O. Löwdin, Rev. Mod. Phys. **34**, 520 (1962).
[29] This expression for L_1 corresponds to the $(1,N-1)$ arrangement of the N-electron Wigner molecule. The $(0,N)$ arrangement is found to be the global ground state for a limited range of values of the fractional filling factor ν near $\nu=1$.
[30] C. Yannouleas and U. Landman (unpublished).
[31] Several different values for ν_0 have been proposed in the literature. Reference 9 determined a value $\nu_0=1/11$. Reference 19 gave a value of $\nu_0=1/7$. Recently, Ref. 12 argued in favor of the value $\nu_0=1/11$.
[32] We remark that, at present, computational difficulties prohibit a straightforward extrapolation of energy to the thermodynamic limit as a function of N and ν. This is the case especially for the disk geometry used here, which is advantageous for studies of crystalline structures, compared to the computationally easier spherical geometry.
[33] P. W. Anderson, *Basic Notions of Condensed Matter Physics* (Addison-Wesley, Reading, MA, 1984), in particular pp. 44–47.
[34] See p. 44 of Ref. 33.
[35] C. Yannouleas and U. Landman, Phys. Rev. Lett. **85**, 1726 (2000).
[36] For the subtleties of calculating in the presence of confinement the edge current from wave functions restricted in the lowest Landau level, see R. Rajaraman and S. L. Sondhi, Mod. Phys. Lett. B **8**, 1065 (1994).
[37] W. Pan, H. L. Stormer, D. C. Tsui, L. N. Pfeiffer, K. W. Baldwin, and K. W. West, Phys. Rev. Lett. **88**, 176802 (2002).
[38] L. Pfeiffer and K. W. West, Physica E (Amsterdam) **20**, 57 (2003).
[39] We remark, however, that the stabilization energy and the gap Δ diminish as the magnetic field increases (see Figs. 6 and 8), and as a result the impurities become more efficient in influencing the WM for the lower fractional fillings (i.e., higher angular momenta).